# AN ADVANCED N-BODY MODEL FOR INTERACTING MULTIPLE STELLAR SYSTEMS
## (USING SWIFT AND WD CODES)

Miroslav Brož[1]

Astronomical Institute of the Charles University, Faculty of Mathematics and Physics,
V Holešovičkách 2, CZ-18000 Praha 8, Czech Republic

## ABSTRACT

We construct an advanced model for interacting multiple stellar systems in which we compute all trajectories with a numerical N-body integrator, namely the Bulirch–Stoer from the SWIFT package. We can then derive various observables: astrometric positions, radial velocities, minima timings (TTVs), minima durations, interferometric visibilities, closure phases, and even complete light curves. We use a modified version of the Wilson–Devinney code for the latter, in which the instantaneous true phase and inclination of the eclipsing binary are governed by the N-body integration. If one has all kinds of observations at disposal, a joint $\chi^2$ metric and an optimisation algorithm (simplex or simulated annealing) allow to search for a global minimum and construct very robust models of stellar systems. At the same time, our N-body model is free from artefacts which may arise if mutual gravitational interactions among all components are not self-consistently accounted for. Finally, we present a number of examples showing dynamical effects that can be studied with our code and we discuss how systematic errors may affect the results (and how to prevent this from happening).

*Keywords:* celestial mechanics — methods: numerical — binaries (including multiple): close, eclipsing — techniques: radial velocities, photometric, interferometric

## 1. INTRODUCTION

Traditional models of eclipsing binaries have to often account for additional external bodies, most importantly as the third light, which makes the depths of primary and secondary minima shallower; light-time effect, causing periodic variations on $O - C$ diagrams; precession of the argument of periastron $\omega$, shifting the secondary minimum due to perturbations by the 3rd body; or changes of inclination with respect to the sky plane, in other words disappearing eclipses.

While analytical theories exist for a description of dynamical perturbations in triple stellar systems and corresponding minima timing variations (also known as TTVs, ETVs; see e.g. Breiter & Vokrouhlický 2015, Borkovits et al. 2016), we would prefer a more general approach — to account for *all* observational data; or at least as much as feasible. So, our aim is to incorporate astrometric or speckle-interferometric positions, radial velocities, minima timings, eclipse durations, spectro-interferometric visibilities, closure phases, and light curves too. At the same time, we do not want to be limited by inevitable approximations of analytical theories (the N-body problem is not integrable) and the only way out seems to be an N-body integrator.

Another aspect is we cannot use analytical photometric models (like those used for exoplanet transits; Mandel & Agol 2002, Carter et al. 2008), because the respective simplifications are not acceptable for stellar eclipses, not speaking about ellipsoidal variations.

In principle, our approach should be rather straightforward: we merge two codes into a single one; namely Levison & Duncan (1974) SWIFT code, and Wilson & Devinney (1971) WD code. In practice, a lot of work has to be done, because both of them have to be modified, we need to extract and derive observable quantities, read observational data and compare them by means of $\chi^2$ statistics. Last but not least, all these computations should be performed in memory, in order to run a minimisation algorithm on top of them.

Even though we do not present new observational data here, there is one recent application of our N-body model to $\xi$ Tauri quadruple system which was described in a great amount of detail in Nemravová et al. (2016). Moreover, there is a comparison with a number of traditional, observation-specific models. In this 'technical' paper, we prefer to show mostly results of numerical simulations, or even negative results contradicting the observations, to demonstrate a sensitivity of our model,

We have a few motivations to do so: (i) no self-consistent N-body model exists yet, which can account for that many observational constraints; (ii) we improved the model significantly compared to Nemravová et al. as we can now model also complete light curves and optionally individual spectra (to be matched by synthetic ones); (iii) the previous paper was a bit lengthy and there was simply not enough room

for a more technical description of our code; (iv) we have to discuss the role of systematics, an experience gained during modelling of real multiple stellar systems.

## 2. MODEL DESCRIPTION

Let us begin with a description of the numerical integrator and the photometric model; then we present a list principal equations and a definition of $\chi^2$ metric used to compare the model with observational data.

### 2.1. *Numerical integrator*

We use the Bulirsch–Stoer numerical integrator, with an adaptive time step, controlled by a unit-less parameter $\epsilon_{\mathrm{BS}}$. The integrator sequentially divides the time step $\Delta t$ by factors 2, 4, 6, ..., checks if the relative difference between successive divisions is less than $\epsilon_{\mathrm{BS}}$ and then performs an extrapolation $\Delta t \to 0$ by means of a rational function (see Figure 1). If the maximum number of divisions $n_{\mathrm{max}} = 10$ is reached, the basic time step $\Delta t$ has to be decreased, with another maximum number of trials $n_{\mathrm{try}} = 30$. We beg to recall this well-known principle here as it is important to always understand principles and limitations of numerical methods in use. This kind of integrator is quite general and there are no restrictions for magnitudes of perturbations, so we can handle keplerian orbits, tiny N-body perturbations or even violent close encounters. Even though it is not symplectic, it does not suffer from an artificial periastron advance.

Apart from the internal time step, a user can choose the output time step $\Delta t_{\mathrm{out}}$. The time stepping was adapted so that we first prepare a list of 'times of interest' (corresponding to all observations) and the integrator outputs coordinates and velocities at exactly these times. Consequently, the need for additional interpolations is eliminated, except for minima timings and minima durations, where a linear interpolation from two close neighbouring points separated by the expected duration is used, and optionally for light curves (see below).

### 2.2. *Photometric model*

The only assumption about geometry of the stellar system, is that only bodies 1 and 2 may be components of an eclipsing binary (or an ellipsoidal variable). Nevertheless, there can be any number of additional bodies, which do contribute to the total light, but we do not compute eclipses for them.

For light curve computations, we use the WD 2005 version, in order to produce compatible and comparable results to Phoebe 1.0, but we plan to upgrade in the future. In brief, the WD code accounts for: black-body radiation or Kurucz atmospheres, bolometric limb darkening, gravity darkening, reflection heating and corresponding thermal emission, axial rotation, or Rossiter–McLaughlin effect. This is a relatively complex photometric model (more complex than analytical models of Mandel & Agol 2002, Carter et al. 2008). We use *no* spots or circumstellar clouds in this version. Usually, the
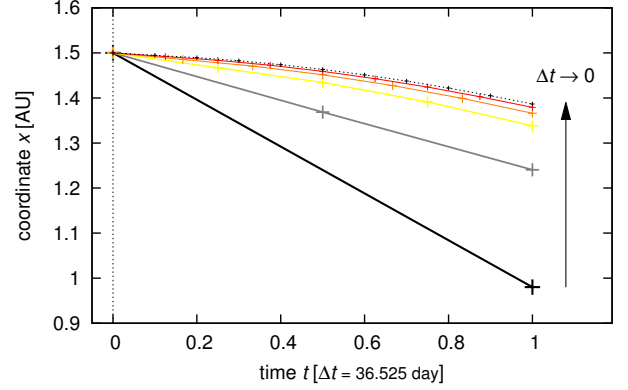


**Figure 1**. A principle of the Bulirsch–Stoer integrator. There is the time $t$ as the independent variable on the abscissa and one of the coordinates $x_{\mathrm{b}}$ on the ordinate. A series of integrations with decreasing time steps $\Delta t_i = \frac{\Delta t}{2}, \frac{\Delta t}{4}, \frac{\Delta t}{6}, \ldots$ is performed and then extrapolated for $\Delta t \to 0$ using a rational function. At the same time, relative differences between successive iterations has to be smaller than $\epsilon_{\mathrm{BS}}$.

code is called with mode 0 (no constraints on potentials) or 2 (luminosity $L_2$ of secondary is computed from temperature $T_2$). Note a number of parameters in lc.in are useless (e.g. orbital elements, precession and period rates, luminosities, potentials etc.) because they are driven from elsewhere.

To speed up light curve computations, we can use a binning of times $\Delta t_{\mathrm{bin}}$ and then linearly interpolate light curve points to the times of observations. For high-cadence data, we can possibly gain a factor of 10 or 100 speed-up this way, but we have to be sure there is no physical process in our model which could change magnitudes on the timescale shorter than $\Delta t_{\mathrm{bin}}$.

### 2.3. *Principal equations*

Principal equations of our N-body model can be summarized as follows: the equation of motion, eclipse detection (including light-time effects), eclipse duration, blackbody approximation, uniform-disk complex visibility, complex triple product, true phase of the eclipsing binary, inclination, and Kopal potential (for the WD code), and synthetic spectrum (with Doppler shifts):[1]

$$\ddot{\mathbf{r}}_{\mathrm{b}i} = -\sum_{j \neq i}^{N_{\mathrm{bod}}} \frac{Gm_j}{r_{\mathrm{b}ji}^3} \mathbf{r}_{\mathrm{b}ji}, \tag{1}$$

$$t'_{\mathrm{ecl}} = t_{\mathrm{min}} + \frac{z_{\mathrm{b}1+2} - z_{\mathrm{b}1+2}(t = T_0)}{c} - \frac{z_{\mathrm{h}2}}{c}, \tag{2}$$

$$\epsilon'_{\mathrm{ecl}} = \frac{2\sqrt{(R_1 + R_2)^2 - \Delta_{\mathrm{min}}^2}}{\bar{v}_{\mathrm{h}2}}, \tag{3}$$

$$L_j(T_{\mathrm{eff}j}, R_j) \doteq \int_{\lambda - \Delta\lambda/2}^{\lambda + \Delta\lambda/2} 4\pi R_j^2 \, \pi B_\lambda(T_{\mathrm{eff}j}) \, \mathrm{d}\lambda, \tag{4}$$

---

[1] The program, including sources and example input data, is available at http://sirrah.troja.mff.cuni.cz/~mira/xitau/.

$$V'(u,v) = \sum_{j=1}^{N_{\text{bod}}} \frac{L_j}{L_{\text{tot}}} 2 \frac{J_1\left(\pi\theta_j\sqrt{u^2+v^2}\right)}{\pi\theta_j\sqrt{u^2+v^2}}\, e^{-2\pi i(ux'_{aj}+vy'_{aj})}, \tag{5}$$

$$T'_3 = V'(u_1,v_1)V'(u_2,v_2)V'(-(u_1+u_2),-(v_1+v_2)), \tag{6}$$

$$\varphi'_{\text{ecl}} = \frac{1}{2\pi}\arctan\frac{\hat{O}\cdot\hat{Y}}{\hat{O}\cdot\hat{X}}, \tag{7}$$

$$i'_{\text{ecl}} = \arccos(-\hat{O}\cdot\hat{Z}), \tag{8}$$

$$\Omega_{\text{Kopal 1 or 2}} = \frac{1}{r_1} + \frac{q}{r_2} + \frac{1}{2}(1+q)r_3^2, \text{ where} \tag{9}$$

$$\begin{cases} r_1 = \frac{R_1}{r_{12}}, r_2 = 1 - r_1, r_3 = r_1, q = \frac{m_2}{m_1}, \text{ or} \\ r_2 = \frac{R_2}{r_{12}}, r_1 = 1 - r_2, r_3 = r_1, \text{ and} \end{cases}$$

$$I'_\lambda = \sum_{j=1}^{N_{\text{bod}}} \frac{L_j}{L_{\text{tot}}} I_{\text{syn}}\left[\lambda\left(1 - \frac{v_{zbj}+\gamma}{c}\right)\right]. \tag{10}$$

The notation for all the quantities is described in Table 1.

Internally, we use a barycentric left-handed Cartesian coordinate system with $x$ negative in the right-ascension direction, $y$ positive in declination, and $z$ positive in radial, i.e. away from the observer; the units are day, au, au/day and $\text{au}^3/\text{day}^2$ for time, coordinated, velocities and masses, respectively. We also need additional coordinate systems, namely: Jacobian (for computations of hierarchical orbital elements), 1-centric (for an eclipse detection), 1+2 photocentric, or 1+2+3 photocentric (for a comparison with astrometric observations of components 3 and 4).

One may immediately note a minor caveat of our model: the geometric radius (in Eq. (3)), the effective radius (in Eq. (4)), the uniform-disk radius (a.k.a. $\theta_j$ in Eq. (5)), and the equatorial radius (used in Eq. (9)) are all assumed to be approximately the same. If this does not hold, it would be necessary to add some three more equations describing relations between them.

## 2.4. Observational data

When we compare our model with observations, we can compute $\chi^2$ for astrometric positions, radial velocities, eclipse timing variations, eclipse duration variations, interferometric squared visibilities, closure phases, triple product amplitudes, light curves, synthetic spectra, and mass constraints (according to spectroscopic classification):

$$\chi^2 = \chi^2_{\text{sky}} + \chi^2_{\text{rv}} + \chi^2_{\text{ttv}} + \chi^2_{\text{ecl}} + \chi^2_{\text{vis}} + \chi^2_{\text{clo}} + \chi^2_{\text{t3}} + $$
$$+ \chi^2_{\text{lc}} + \chi^2_{\text{syn}} + \chi^2_{\text{mass}}, \tag{11}$$

$$(\Delta x_{ji}, \Delta y_{ji}) = \mathbf{R}\left(-\phi_{\text{ellipse}} - \frac{\pi}{2}\right) \times \begin{pmatrix} x'_{p\,ji} - x_{p\,ji} \\ y'_{p\,ji} - y_{p\,ji} \end{pmatrix}, \tag{12}$$

$$\chi^2_{\text{sky}} = \sum_{j=1}^{N_{\text{bod}}} \sum_{i=1}^{N_{\text{sky}\,j}} \left\{ \frac{(\Delta x_{ji})^2}{\sigma^2_{\text{sky major}\,ji}} + \frac{(\Delta y_{ji})^2}{\sigma^2_{\text{sky minor}\,ji}} \right\}, \tag{13}$$

**Table 1.** Notation used for coordinates, velocities, other quantities and uncertainties, which we use in our N-body model.

| | |
|---|---|
| $N_{\text{bod}}$ | number of bodies |
| $m$ | mass ($GM_\odot$ units) |
| $x_{\text{b}}, y_{\text{b}}, z_{\text{b}}$ | barycentric coordinates |
| $v_{x\text{b}}, v_{y\text{b}}, v_{z\text{b}}$ | barycentric velocities |
| $x_{\text{h}}, y_{\text{h}}, z_{\text{h}}$ | 1-centric coordinates |
| $v_{x\text{h}}, v_{y\text{h}}, v_{z\text{h}}$ | 1-centric velocities |
| $x_{\text{p}}, y_{\text{p}}$ | 1+2 photocentric sky-plane coordinates |
| $x_{\text{p3}}, y_{\text{p3}}$ | 1+2+3 photocentric coordinates |
| $x_{\text{a}} = \frac{x_{\text{h}}}{d}, y_{\text{a}}$ | 1-centric coordinates in an angular measure |
| $\hat{X}, \hat{Y}, \hat{Z}$ | unitvectors aligned with 1+2 eclipsing pair |
| $\hat{O} = (0,0,-1)$ | observers direction |
| $\gamma$ | systemic velocity |
| $v_{\text{rad}}$ | observed radial velocity |
| $t_{\text{ecl}}$ | mid-epoch of an eclipse of 1+2 pair |
| $\epsilon_{\text{ecl}}$ | eclipse duration |
| $V$ | complex visibility, squared visibility is $|V|^2$ |
| $T_3$ | complex triple product, closure phase is $\arg T_3$ |
| $u, v$ | projected baselines (expressed in cycles, $\frac{B}{\lambda}$) |
| $\theta = \frac{2R}{d}$ | angular diameter |
| $d$ | distance to the system |
| $L, L_{\text{tot}}$ | component luminosity and the total one |
| $T_{\text{eff}}$ | effective temperature |
| $R$ | stellar radius (uniform-disk) |
| $\lambda, \Delta\lambda$ | effective wavelength and bandwidth |
| $B_\lambda(T)$ | the Planck function |
| $m_V$ | magnitude (in V band or another) |
| $I_\lambda$ | normalized monochromatic intensity |
| $\sigma_{\text{sky major, minor}}$ | uncertainty of the astrometric position, angular sizes of the uncertainty ellipse |
| $\phi_{\text{ellipse}}$ | position angle of the ellipse |
| $\mathbf{R}(\dots)$ | the corresponding $2\times 2$ rotation matrix |
| $\sigma_{\text{rv}}$ | uncertainty of the radial velocity |
| $\sigma_{\text{ttv}}$ | uncertainty of the eclipse mid-epoch timing |
| $\sigma_{\text{ecl}}$ | uncertainty of the eclipse duration |
| $\sigma_{\text{vis}}$ | uncertainty of the squared visibility |
| $\sigma_{\text{clo}}$ | uncertainty of the closure phase |
| $\sigma_{\text{t3}}$ | uncertainty of the triple product amplitude |
| $\sigma_{\text{lc}}$ | uncertainty of the light-curve data |
| $\sigma_{\text{syn}}$ | uncertainty of the normalized intensity |
| $m_j^{\text{min}}, m_j^{\text{max}}$ | minimum and maximum masses |

$$\chi^2_{\text{rv}} = \sum_{j=1}^{N_{\text{bod}}} \sum_{i=1}^{N_{\text{rv}\,j}} \frac{\left(v'_{zb\,ji} + \gamma - v_{\text{rad}\,ji}\right)^2}{\sigma^2_{\text{rv}\,ji}}, \tag{14}$$

$$\chi^2_{\text{ttv}} = \sum_{i=1}^{N_{\text{ttv}}} \frac{(t'_{\text{ecl}\,i} - t_{\text{ecl}\,i})^2}{\sigma^2_{\text{ttv}\,i}}, \tag{15}$$

$$\chi_{\text{ecl}}^2 = \sum_{i=1}^{N_{\text{ecl}}} \frac{(\epsilon'_{\text{ecl}\,i} - \epsilon_{\text{ecl}\,i})^2}{\sigma_{\text{ecl}\,i}^2}, \tag{16}$$

$$\chi_{\text{vis}}^2 = \sum_{i=1}^{N_{\text{vis}}} \frac{\left(|V'(u_i, v_i)|^2 - |V|_i^2\right)^2}{\sigma_{\text{vis}\,i}^2}, \tag{17}$$

$$\chi_{\text{clo}}^2 = \sum_{i=1}^{N_{\text{clo}}} \frac{(\arg T'_{3i} - \arg T_{3i})^2}{\sigma_{\text{clo}\,i}^2}, \tag{18}$$

$$\chi_{\text{t3}}^2 = \sum_{i=1}^{N_{\text{t3}}} \frac{(|T_{3i}|' - |T_{3i}|)^2}{\sigma_{\text{t3}\,i}^2}, \tag{19}$$

$$\chi_{\text{lc}}^2 = \sum_{k=1}^{N_{\text{band}}} \sum_{i=1}^{N_{\text{lc}\,k}} \frac{(m'_{Vki} - m_{Vki})^2}{\sigma_{\text{lc}\,ki}^2}, \tag{20}$$

$$\chi_{\text{syn}}^2 = \sum_{i=1}^{N_{\text{syn}}} \frac{(I'_{\lambda\,i} - I_{\lambda\,i})^2}{\sigma_{\text{syn}\,i}^2}, \tag{21}$$

$$\chi_{\text{mass}}^2 = \sum_{j=1}^{N_{\text{bod}}} \left(\frac{2m_j - m_j^{\min} + m_j^{\max}}{m_j^{\max} - m_j^{\min}}\right)^{100}. \tag{22}$$

Again, the quantities are described in Table 1. The index $i$ always corresponds to observational data, $j$ to individual bodies, and $k$ to sets of data. The dashed quantities correspond to synthetic data, integrated (or interpolated) to the times of observations $t_i$.

To find a local or a global minimum, we can use a standard simplex algorithm or simulated annealing (Press et al. 1997), with the cooling schedule $T^{i+1} = (1 - \epsilon_{\text{temp}})T^i$, after given number of iterations at $T^i$. Free parameters of the model (which can be optionally fixed) are: masses $m_j$ of the components, orbital elements $a_j, e_j, i_j, \Omega_j, \omega_j, M_j$ of the respective orbits, systemic velocity $\gamma$, distance $d$, radii $R_j$, and effective temperatures $T_{\text{eff}\,j}$. For $N_{\text{bod}}$ bodies, this represents a set of $(9N_{\text{bod}} - 4)$ parameters in total.

As usually, observational data have to be in a suitable format and we provide some example scripts for a conversion or extraction of data from OIFITS files (Pauls et al. 2005). Note that one shall *not* use the triple product amplitude $|T_3|$ when the same interferometric measurements are used as the squared visibility $|V|^2$. Similarly, no minima timings or durations are needed when we have complete light curves at disposal (cf. Figure 2); and no RV measurements when we fit the observed spectra with synthetic ones.

## 3. EXAMPLES OF DYNAMICAL EFFECTS

To demonstrate some capabilities of our N-body model we present several numerical simulations that can be treated as examples of what can be fitted to observational data (more examples can be found in Fabrycky et al. 2010).
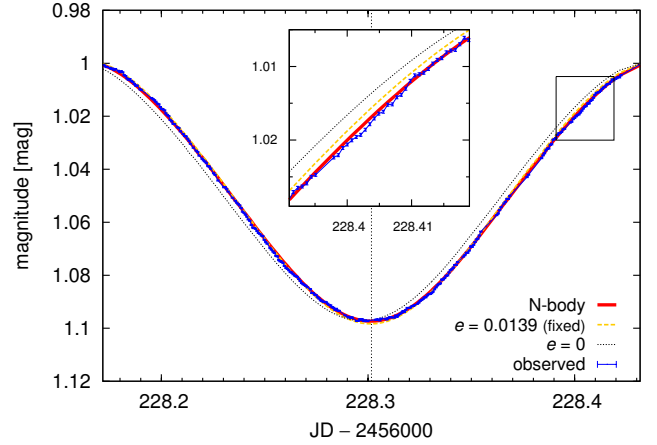


**Figure 2**. Light curves of a detached eclipsing binary and three dynamical models: (i) a keplerian (2-body) assuming a fixed circular orbit ($e = 0$, black dotted line), (ii) a keplerian with a non-zero fixed eccentricity $e = 0.0139$ (yellow), and (iii) an N-body with the initial osculating $e_1(t = T_0) = 0$ (red), but with a general trajectory affected by perturbations among four components. The last case corresponds to the arrangement of $\xi$ Tauri quadruple system (as described in Nemravová et al. 2016). The light curves and minima timings differ more than the usual uncertainty $\sigma_{\text{ttv}}$, or $\sigma_{\text{lc}}$ achievable by space-born observations like that of MOST (Walker et al. 2003; cf. blue line with tiny error bars). It is thus necessary to use the N-body model for such compact stellar systems, even on this *very short* (orbital) time scale.

### 3.1. *Precession of $\omega$ and $\Omega$*

Probably the most trivial perturbation is the precession of the argument of pericentre $\omega$. In our case however, the temporal derivative $\dot{\omega}$ is *not* a free parameter; it is directly tied to the masses and initial osculating elements of the bodies. The same holds for the longitude of the ascending node $\Omega$ and the corresponding $\dot{\Omega}$. It is thus not necessary to use any secular theories, because all secular perturbations are implicitly included in our N-body model. Moreover, one can expect that neither $\dot{\omega}(t)$ nor $\dot{\Omega}(t)$ are constants, but some short-periodic perturbations are always present.

Depending on the distribution of the angular momentum $\mathbf{L}$ in the system, the precession of individual orbits can occur with different amplitudes, although the secular time scales for a pair of orbits are the same. In the Laplace coordinate system (aligned with total $\mathbf{L}$), all $\bar{\omega}_j$ and $\bar{\Omega}_j$ circulate from 0 to $360°$. On the other hand, our frame of reference is tied to the observers direction and the sky plane, so that $\omega_j$ or $\Omega_j$ often *librate*, in other words oscillate in a limited interval of values, due to a purely geometrical projection.

### 3.2. *Inclination vs eclipse durations*

As a result of the nodal precession $\dot{\Omega}_j$ of each orbit, the inclinations $i_j$ with respect to the sky plane also often librate. Regarding the case of $i_1$, the eclipsing binary may exhibit one or more photometric effects: changes of eclipse durations, eclipse depths, or completely disappearing (and then reappearing) eclipses. All of these are accounted for and contribute to $\chi_{\text{ecl}}^2$, $\chi_{\text{lc}}^2$, or $\chi_{\text{ttv}}^2$ terms.
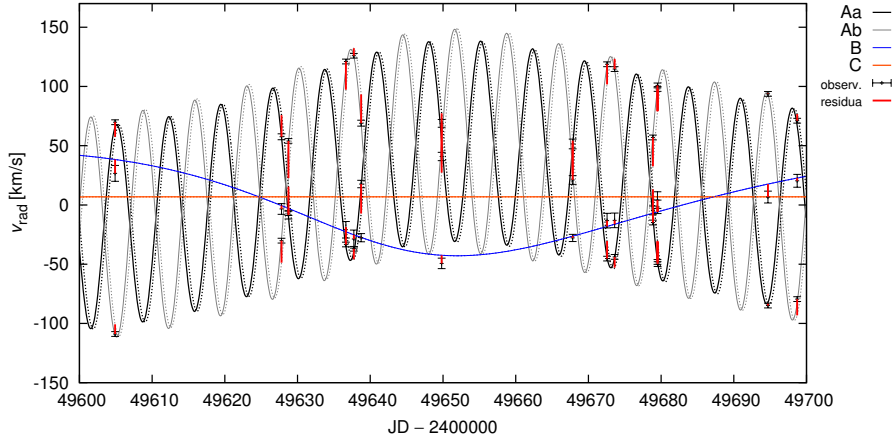
**Figure 3**. An evolution of radial velocities (RVs) of the four components of $\xi$ Tauri (denoted Aa, Ab, B and C), assuming two different values of the initial osculating eccentricity $e_1(t = T_0)$: (i) zero (thick lines); (ii) an increased non-zero $e_1 = 0.01$ (dotted lines). There is a significant phase shift between them, when can be easily detected because the respective RV measurements cover the interval of JD from 2449300 to 2456889. For even larger $e_1 \simeq 0.1$, the oscillations of RVs forced by the 3rd body also have larger amplitude, related to the evolution of $e_1(t)$. For comparison, there are some of the observations plotted (black points with error bars) and residua wrt. the worse non-zero $e_1$ model (red lines).

Our model is also extremely sensitive to the *mutual* inclination $J$ of the orbits, because the precession rates are functions of it (see Eqs. 26 and 27 in Nemravová et al. 2016, but these are suitable only for low $e_1$, low $J$ and large $a_2/a_1$). This may significantly contribute to $\chi^2_{\rm sky}$, or $\chi^2_{\rm vis}$.

### 3.3. *Eccentricity oscillations*

Yet another phenomenon may occur on secular time scales, namely oscillations of the osculating eccentricity $e_1(t)$ forced by the 3rd body. In an 'extreme' case, $e_1(t = T_0) \simeq 0.1$, it is manifested as forced oscillations of radial velocities which no longer have constant amplitude.

For low eccentricities of the order of $0.01$, one can search for some phase shifts of RVs of components 1 and 2. This turns out to be a strong constraint for the initial eccentricity $e_1(t = T_0)$, because the phase shifts occur as soon as $e_1 \neq 0$. An example for $\chi$ Tau system is shown in Figure 3.

### 3.4. *Variation and evection*

Apart from secular perturbations, there are short-periodic perturbations which occur on the *orbital* time scales $P_j$ of the individual orbits. In a classical Hills theory, we would have five terms contributing to departures of the true longitude $\Delta\lambda$ (Fitzpatrick 2012): eccentricity, ellipticity, inclination, variation and evection. The last two are of interest, as they arise from interactions with the external 3rd body. One can recognise the variation is maximal in octant points, and the evection in quadrant points (wrt. to the 3rd body).

In Figure 4 we demonstrate these short-periodic effects for a system similar to $\xi$ Tau. In this example, however, we increased the eccentricity $e_1 = 0.01$, so that the evection is not zero. Note the 3rd may be practically 'fixed' and still cause variation or evection which contribute mostly to $\chi^2_{\rm rv}$, but not directly to $\chi^2_{\rm ttv}$, since the eclipses are always measured at the
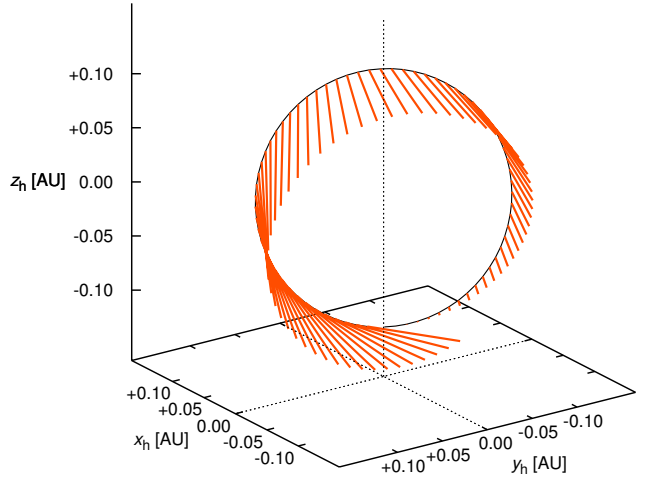


**Figure 4**. A general trajectory of the inner eclipsing binary as output from our N-body model, affected by the 3rd and 4th component in $\xi$ Tauri quadruple system. The differences (orange lines) with respect to a keplerian orbit (black curve) — fixed at the initial conditions — were exaggerated 100 times to make them visible at all. Two most important terms describing departures in longitude $\Delta\lambda$ are called the variation and evection.

same true longitude $\lambda$.

### 3.5. *Prograde vs retrograde orbits*

Traditionally, it is practically impossible to distinguish prograde and retrograde orbits, because the corresponding RVs are the same. But luckily, mutual interactions within the N-body model can contribute to $\chi^2_{\rm ttv}$ sufficiently (cf. Fig. 12 in Nemravová et al. 2016). The principle is as follows: if the distance of the 3rd body is increasing (or decreasing) during one $P_1$, the gravitational potential at around the binary is less negative (or more) and consequently the value of $P_1$ is inevitably larger (smaller).
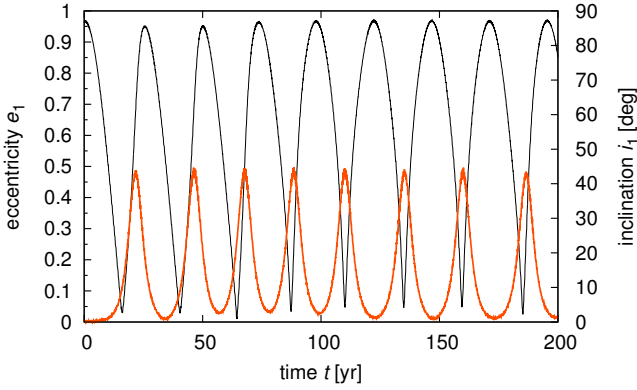
**Figure 5**. Kozai cycles in a hypothetical quadruple system with the mutual inclination $J = 50°$ of the first two orbits, i.e. larger than the critical value $i_{\min}$. The coupled oscillations of the eccentricity $e_1$ (orange) and inclination $i_1$ (black) would be visible, on the time scale as short as $T_{\mathrm{Kozai}} \simeq 19\,\mathrm{yr}$.

### 3.6. *Kozai cycles*

It we turn our attention to long-periodic effects, one classical example are Kozai cycles (Kozai 1962), or coupled oscillations of the eccentricity $e$ and inclination $i$ which preserve the invariant $L_z = \sqrt{1 - e^2}\cos i$. They occur for high-inclination orbits with a certain minimum (critical) inclination $i_{\min}$.

We can easily demonstrate such oscillations, if we substantially increase the mutual inclination $J$ in $\xi$ Tau system (see Figure 5). However, in this particular case the system is so massive and compact that the approximations involved in the derivation of $L_z$ integral do not hold anymore! The respective time scale ($19\,\mathrm{yr}$) of the oscillations is also shorter than predicted by the analytical theory; and there is a 4th body with a $51\,\mathrm{yr}$ orbit involved, so that the phasing of $e$, $i$ is not exact.

### 3.7. *Long-term evolution and stability*

It is also possible to run the N-body integrator separately, regardless of observational time span, and study a long-term evolution and stability of stellar systems. One of the difficulties is that and the output of osculating elements is either prohibitively long or an *aliasing* occurs when the output time step $\Delta t_{\mathrm{out}}$ is larger than an half of the shortest orbital period, $P_1/2$.

In a modified version of the BS integrator (swift_bs_fp), we can use on-line digital filtering of non-singular osculating elements $h_j, k_j, p_j, q_j$ to overcome these problems: first a multi-level convolution based on Kaiser windows (Quinn et al. 1991) to obtain *mean* elements, and second a frequency-modified Fourier transform (Šidlichovký & Nesvorný 1997) to extract *proper* elements. For $N$ mutually interacting bodies, one can expect $2N$ eigen-frequencies of the system, which are usually denoted $g_j$ and $s_j$. The corresponding amplitudes $e_{\mathrm{p}j}, \sin\frac{1}{2}I_{\mathrm{p}j}$ can be considered approximate integrals of motion which only evolve on long time scales (longer
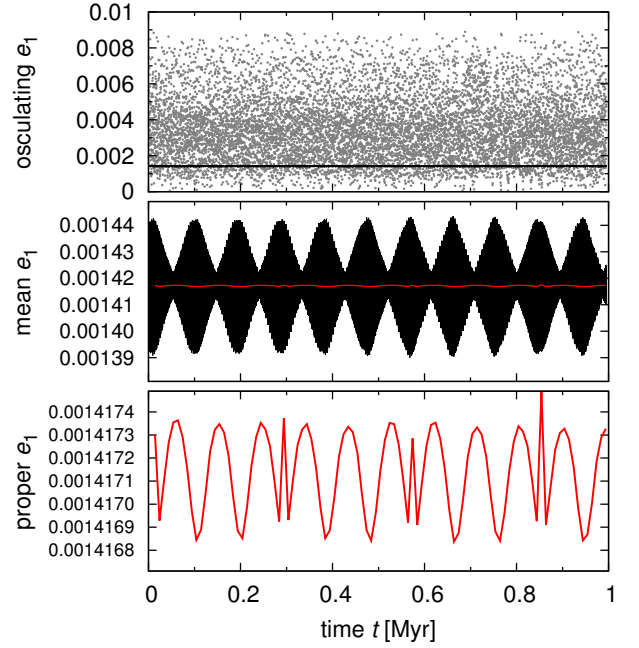


**Figure 6**. A long-term evolution of $\xi$ Tauri quadruple system, or the eccentricity $e_2(t)$ of the 2nd orbit, respectively. There are osculating (top), mean (middle), and proper (bottom) orbital elements shown. Note the osculating elements may exhibit aliasing, i.e. artificial long-period changes, because the sampling $\Delta t_{\mathrm{out}} = 100\,\mathrm{yr}$ is limited and the corresponding Nyquist period is $P_{\mathrm{Ny}} = \Delta t_{\mathrm{out}}/2$.

than secular; see Figure 6).

### 3.8. *Close encounters*

Additionally, one can model also hyperbolic trajectories and three-body encounters or captures, even though from a historical perspective such stellar models do not seem very convincing (Tokovinin 1986), because some observations may be affected by raw measurement errors (e.g. a wrong plate scale), a change of the orbital period may turn out to be rather quasiperiodic (possibly related to magnetic phenomena) and any interstellar encounter is considered a too rare event.

Finally, let us mention that all mean-motion resonances (Rivera et al. 2005), secular resonances, tree-body resonances (Nesvorný and Morbidelli 1998), or chaotic diffusion due to overlapping resonances are also naturally accounted for in our N-body model.

### 4. POSSIBLE PROBLEMS DUE TO SYSTEMATICS

We have to admit that any modelling (compact stellar systems included) can be spoiled, either when there are systematic deficiencies of the model, e.g. keplerian vs N-body, or serious systematic errors in observational data, especially when we use very heterogeneous datasets. In the following, we thus discuss several 'dangerous' cases.

### 4.1. *Discretisation errors*

Of course, any numerical computation suffers from discretisation errors and interpolation errors, even thought we tried to decrease the latter as much as possible (cf. Section 2). This is probably the most important disadvantage compared to analytical computations. A general rule is a convergence of results (and corresponding $\chi^2$ values) for $\Delta t \to 0$.

However, let us add a warning that rarely a decrease of time step, e.g. by a factor of 2, may lead to unexpected results. For example, when eclipses are almost disappearing, the trajectory with $\Delta t/2$ is more curved and may thus miss the last eclipse, which suddenly *increases* the $\chi^2_{\text{ttv}}$ because the next eclipse is now one orbital period $P$ far away.

Let's not forget, there is yet another discretisation related to the WD code, or the surfaces of the eclipsing binary. For low numbers $N_{\text{wd}}$, one can see numerical artefacts on the light curve, as the rectangular surface facets appear from behind the limb, or disappear. Again, it is worth to check larger $N_{\text{wd}}$.

### 4.2. *Mirror solutions*

Sometimes we can expect one or more ($m$) mirror solutions (and $2^m$ combinations of them). A typical situation is we have no RVs for faint components (so that both inclinations $i$ and $i' = -i$ are admissible), or no unambiguous astrometry or closure-phase measurements (so that $\Omega$ and $\Omega' = 180° - \Omega$ are both admissible).

However, with our N-body model it is worth to check not only the total $\chi^2$ but also individual components of $\chi^2$; especially $\chi^2_{\text{ttv}}$ is very sensitive to the mutual perturbations. Of course, it must not be spoiled by systematics or strongly underestimated uncertainties in other observational data. If this is the unfortunate case, one may try to use weights $w$ of individual $\chi^2$'s, but this should be used as "a method of a last resort". The reason is that it is too easy to hide *all* systematics this way, even though it is better to get rid of them (see below).

### 4.3. *Heterogeneous datasets of RVs*

Radial-velocity measurements might be affected by zero point offsets, which then lead to different systemic velocities $\gamma$ for different observatories. This can be a bit misleading, because it is not possible to *a-priori* distinguish systematic differences in dispersion relations from real perturbations, when the observations were acquired at epochs distant in time.

A well-known approach is to use an independent calibration by narrow interstellar lines (DIBs; Chini et al. 2012), if they are present and resolved in the given spectral range. If this is impossible, one should use the N-body model with a great caution, because simply increasing $\sigma_{\text{v}} \simeq \Delta\gamma$, to get $\chi^2_{\text{rv}} \simeq N_{\text{rv}}$ is an apparently wrong idea. The RV measurements in question will still 'push' the model elsewhere and there will be systematic departures wrt. other (more or less orthogonal) observational data.

It may be a too much freedom, but if the dispersion relations can be considered stable from night to night, some calibration factors $f_{\text{rv}\,k}$ of RVs — assigned to individual observatories or datasets — might be actually a better solution. In any case, such factors have to be always treaded as additional free parameters of the N-body model.

### 4.4. *RVs from disentangling*

Another possibility is to derive RVs in the Fourier domain, by means of disentangling (e.g. by Korel; Hadrava 2009). Moreover, there is an advantage in obtaining disentangled spectra of individual components. In case of this method, one can expect a strong correlation of RVs and the fixed keplerian orbital elements used during the disentangling procedure. This represents a problem, because we do vary initial osculating orbital elements in the N-body model and they most likely will contradict the previous elements.

Note the disentangled spectra should *not* be re-used as templates, because they contain slight systematic asymmetries or wavy continua. If we try to match the observed spectra with these templates again, we would obtain artificially small uncertainties $\sigma_{\text{rv}}$ (and extremely large $\chi^2_{\text{rv}}$). A solution is to use synthetic spectra similar to the disentangled ones, but with no direct relation to Korel, as an intermediate step to derive new RVs.

### 4.5. *RVs from synthetic spectra*

Alternatively, RVs of the individual components can be derived directly in the time domain by fitting a luminosity-weighted sum of suitable synthetic spectra (e.g. by Pyterpol; Nemravová et al. 2016). Instead of fitting the observed spectra individually (one-by-one), it is advisable to assume that most of the free parameters (projected $v_{\text{rot}\,j}$, $T_{\text{eff}\,j}$, $\log g_j$ of the stellar components) are the same for all spectra, with the exception of RVs which are surely time dependent. Luckily, these RVs are *not* strongly correlated with the orbital elements, so they seem suitable as an input for an N-body model.

On the other hand, this method can have problems when RVs are small (at conjunctions) and $v_{\text{rot}}$ large, so that the lines are totally blended. As a provisional solution, one may try to discard the lowest RVs which cause the problems, or do *not* use RVs at all and rather fit synthetic spectra directly with the N-body model, which is definitely a better approach, because RVs will be correctly tied to each other.

### 4.6. *Rectification procedure*

Inevitably, RVs might be systematically affected already during a basic reduction, namely a rectification (normalisation) of spectra. If the rectification procedure is automated by fitting a low-degree polynomial to continua, it is worth to try a different maximum degree of the polynomial and run the above synthetic spectra optimisation once again.

### 4.7. *Visibility calibration*

Contrary to closure phase $\arg T_3$ measurements, the squared visibility $|V|^2$ has to be calibrated by close-in-time observations of comparison stars with known angular diameters or unresolved (point-like) sources. Sometimes even the calibrated measurements exhibit unrealistically quick changes of $|V|^2$ or sudden decreases of $|V|^2$, possibly caused by unfavorable weather conditions, or seeing comparable to the slit width, affecting a light contribution from barely-resolved components, or other instrumental defects.

In the end, dropping of these suspicious observational data may be the only way to prevent the systematics to unrealistically 'push' the model. Using a low weight $w_{\mathrm{vis}} = 0.1$ is not a satisfactory option. To this point, we always retain a dataset identification for each single measurement which enables us to 'quickly' perform a bootstrap testing.

### 4.8. *Quasiperiodic oscillations*

A removal of quasiperiodic oscillations which are sometimes (or rather always) present outside eclipses is very important, because it may otherwise systematically offset the minima timings themselves. One wave of the oscillations behaves like a 'ramp', which skews the light curve at around the minimum.

The observed light curve should be thus *locally* fitted by a suitable function (e.g. harmonic with a variable period and amplitude) and then subtracted from the data. If the (synthetic) light curve out of eclipses is flat beyond doubt, it seems better to drop these segments of the (observed) light curve, because they increase $\chi^2_{\mathrm{rc}}$ and there is no useful information as we have no physical model for these oscillations.

### 4.9. *Osculating vs fixed elements*

Some care is needed when comparing results of (old) keplerian and (new) N-body models. They actually *can* differ by more than a few $\sigma$, because the former orbital elements are fixed, while the latter are only osculating initial conditions at $t = T_0$. Generally, all elements are time-dependent quantities, $a_1(t), e_1(t), i_1(t)$, etc., where the oscillations are often *larger* than the uncertainties of the initial osculating elements. In fact, one can perform some averaging over the observational time span. Nevertheless, the N-body model is more complete, and it should be probably preferred.

### 4.10. *Jacobian osculating elements*

Unlike the usual stellar-astronomy convention, where the brightest component is always at the origin of the reference frame, in our N-body model we usually select the most compact eclipsing pair as bodies 1 and 2, or the most massive component as 1. The reason is that orbital elements in hierarchical systems are usually computed in Jacobian coordinates, where the centre of mass 1+2 is the reference point for the coordinates and velocities of the 3rd body; the 1+2+3 centre of mass is a suitable reference for the 4th body, and so on. The corresponding Jacobian elements then have a nice interpretation.

Because of the above definition, it may be necessary to adjust to-be-fitted astrometric measurements by $180°$ in the position angle — not due to an ambiguity, but simply because the reference body is different in our case. Similarly, a value of $\Omega$ from literature may actually differ by $180°$.

To conclude in a pessimistic way, the above list of possible problems and systematics cannot be treated as complete, unfortunately.

### 5. CONCLUSIONS AND FUTURE WORK

Today, N-body models seem to be absolutely necessary tool for a careful inspection of observational data. It is important to take care that discrepancies between keplerian and full N-body dynamics no longer spoil derived stellar parameters. After a removal of (some) systematic errors (sometimes) present in observations or reductions, it enables us to reveal even tiny N-body perturbations and construct robust models of compact stellar systems.

Regarding future developments of (our or other) N-body models, it seems to be worthwhile to also account for: calibration factors of individual interferometric telescopes, limb darkening in the visibility calculation, especially when measuring on longest baselines, general-relativistic precession in some cases, and eventually one may think of an upgrade to the WD 2015, or Phoebe 2.0.

Yet another work is needed to compute trajectories even more accurately, with physics going beyond point-like masses, namely: gravitational moments $J_2$, $J_4$ due to non-sphericity of stellar components, tidal interactions, corresponding long-term circularisation of orbits, Kozai cycles with tides, spin–orbital resonances, or radiation of gravitational waves in extreme cases.

### REFERENCES

Borkovits, T., Hajdu, T., Sztakovics, J., et al. 2016, MNRAS, 455, 4136

Breiter, S. & Vokrouhlický, D. 2015, MNRAS, 449, 1691

Carter, J. A., Yee, J. C., Eastman, J., et al. 2008, ApJ, 689, 499

Chini, R., Hoffmeister V. H., Nasseri, et al. 2012, MNRAS, 424, 1925

Fabrycky, D. C. 2010, Non-Keplerian Dynamics, in Exoplanets, ed. S. Seager, University of Arizona Press

Fitzpatrick, R. 2012, An Introduction to Celestial Mechanics, Cambridge University Press

Kozai, I. 1962, AJ, 67, 591

Mandel, K. & Agol, E. 2002, ApJ, 580, 171

Nemravová, J., Harmanec, P., Brož, M., et al. 2016, A&A, submitted

Nesvorný, D. & Morbidelli, A. 1998, AJ, 116, 3029

Levison, H. F. & Duncan, M. J. 1994, Icarus, 108, 18

Pauls, T. A., Young, J. S., Cotton, W. D. & Monnier, J. D. 2005, PASP, 117, 1255

Quinn, T. R., Tremaine, S. & Duncan, M. 1991, AJ, 101, 2287

Rivera, E. J., Lissauer, J. J., Butler, R. P., et al. 2005, ApJ, 634, 625

Šidlichovský, M. & Nesvorný, D. 1996, CeMDA, 65, 137

Tokovinin, A. A. 1986, Astronomicheskii Tsirkulyar, 1415, 1

Walker, G., Matthews, J., Kuschnig, R., et al. 2003, PASP, 115, 1023

Wilson, R. E & Devinney, E. J. 1971, ApJ, 166, 605